受入
81-1-27
高エネ研図書室

CERN - DATA HANDLING DIVISION
DD/80/3
February 1980

FILTERS FOR THREE-DIMENSIONAL LIMITED ANGLE TOMOGRAPHY

B. Schorr,

DD Division, CERN, Geneva,

Switzerland,

and

D. Townsend,

Dept. of Nuclear Medicine,

Cantonal Hospital, Geneva,

Switzerland.

(Submitted to the Journal of Computer Assisted Tomography)

FILTERS FOR LIMITED ANGLE TOMOGRAPHY

ABSTRACT

Tomographic reconstruction from projections has been studied for the case where projections are available within only a limited angular range. This situation is of interest in transmission computerized tomography (CT) with the desire to reduce patient radiation dose and decrease scan time, but is of particular interest in emission CT employing a dual-detector, large area, stationary positron camera. Efficient usage of the data from such a camera requires full, three-dimensional reconstruction with the restricted range of projections viewed by the imaging system. One such reconstruction algorithm, based on back-projection with subsequent frequency space filtering, has been considered, and the derivation of analytic expressions for the appropriate filters corresponding to four possible point response functions is given. The effectiveness of the filters for deconvolution is demonstrated for some computer-simulated images.

Terms: Positron emission tomography - Emission computed tomography - Limited angle reconstruction - Three-dimensional deconvolution.

1. INTRODUCTION

The X-ray transmission scanner, by combining information from a series of one-dimensional projections, is able to reconstruct the distribution of linear attenuation coefficients for a two-dimensional, transverse cross-section of the human body. Usually, the projection angles are distributed uniformly through 360°, with a spacing that depends upon the resolution required in the final image. Interest in reconstructions where the projection angles are limited to a range of less than 360° stems from the desire to reduce both the scan time and the dose delivered to the patient, while maintaining an image resolution adequate for diagnosis.

The imaging information in emission tomography comes from photons emitted by a radioactive source distributed within the patient. Interest in limited angle reconstructions arises in this case from restrictions imposed by the geometry of the imaging system. Since the photons are emitted isotropically into the full solid angle, the dose delivered to the patient is clearly independent of the number and angular distribution of the projections actually measured. Maximum use of the available information is obviously made by covering as much of the full solid angle as practically possible. No imaging system offers complete coverage, and, in nuclear medicine, detection is usually limited to photons from a single direction incident on a large area, position-sensitive detector. Although the detector (e.g. an Anger camera) is sensitive to photons from any direction within its acceptance angle, restriction to only one direction, by means of a lead collimator, is necessary to form a meaningful projection of the radionuclide distribution. The multiple projections required for tomography are obtained by rotating this system through one complete revolution[1)], or by rotating a pair of such detectors through half a

revolution[2]. Reconstruction methods analogous to those for X-ray transmission tomography[3] are then used to produce a series of two-dimensional transverse sections mapping the internal radionuclide distribution.

An obvious disadvantage of the above system is the need to limit the direction of the incident photons to form a meaningful image, thereby reducing considerably the potential sensitivity of the camera. This drawback is overcome with the use of positron-emitting radionuclides, where, instead of the emission of a single photon, the radioactive decay releases a positive electron[4]. The two photons that are created by the subsequent positron-electron annihilation are emitted 180° apart, so that detection of this photon pair in coincidence defines a direction (see fig. 1). The directional restrictions of single-photon emission may now be relaxed, accepting all incident photons and resorting into specific projections at a later time.

The rotation of a dual detector system operating in coincidence collects sufficient projection information for a complete tomographic reconstruction[5], providing the angle of rotation is at least 180°. Additional projections are redundant except in as far as they help reduce statistical error. When the rotational angle is less than 180° or, more likely, the detector system is stationary, limited angle reconstruction is necessary[6].

The most commonly used reconstruction methods are variations of the filtered-back projection approach[7,8], with the filtering usually performed in Fourier space. Determination of the appropriate frequency-space filter is therefore a prerequisite of the reconstruction. The image obtained by simple back-projection[5] of the projection data may be expressed as a convolution of the unknown radionuclide distribution with the point

response function of the imaging system[9], so that the corresponding frequency-space filter is the Fourier transform of this response function.

This paper will describe the derivation of a class of filters appropriate for limited angle reconstruction based on back-projection with filtering. For completeness, an outline of the reconstruction method will be given in the next section, and the choice of a suitable point response function is discussed in section 3. Section 4 covers the derivation of the filters, and in section 5 some reconstructions for computer-simulated images are presented.

2. FOURIER DECONVOLUTION

The unmodified, simple back-projection of a series of projections obtained by imaging a single point, yields a function that represents the system response to a point source. If simple back-projection gave a true reconstruction, the point response function would also be a point, but this is of course not the case. In two dimensions, for section imaging, the system point response function (p.r.f.) varies as the inverse distance from the point source, while in three-dimensions the p.r.f. varies as the inverse square of this distance[10]. Assuming this function is invariant of the position of the point source within the field of view of the imaging system, the result of imaging an unknown, extended distribution $f(x,y,z)$ and then back-projecting the unmodified projections can be expressed as a convolution of $f(x,y,z)$ with the invariant p.r.f., $h(x,y,z)$ [9]:

$$\hat{f}(x,y,z) = \int_{-\infty}^{\infty}\int_{-\infty}^{\infty}\int_{-\infty}^{\infty} f(x',y',z')\, h(x-x',y-y',z-z')\, dx'\, dy'\, dz' \,, \qquad (1)$$

where $\hat{f}(x,y,z)$ is the image estimate from simple back-projection. The most elegant way to solve eq. (1) for the unknown function $f(x,y,z)$ is to use the Fourier convolution theorem in three-dimensions, so that the convolution reduces to a point-wise product:

$$\hat{F}(k_x,k_y,k_z) = F(k_x,k_y,k_z)\ H(k_x,k_y,k_z)\ , \tag{2}$$

where

$$\hat{F}(k_x,k_y,k_z) = \int_{-\infty}^{\infty}\int_{-\infty}^{\infty}\int_{-\infty}^{\infty} \hat{f}(x,y,z)\ e^{-2\pi i(xk_x+yk_y+zk_z)}\ dx\ dy\ dz \tag{3a}$$

$$F(k_x,k_y,k_z) = \int_{-\infty}^{\infty}\int_{-\infty}^{\infty}\int_{-\infty}^{\infty} f(x,y,z)\ e^{-2\pi i(xk_x+yk_y+zk_z)}\ dx\ dy\ dz \tag{3b}$$

$$H(k_x,k_y,k_z) = \int_{-\infty}^{\infty}\int_{-\infty}^{\infty}\int_{-\infty}^{\infty} h(x,y,z)\ e^{-2\pi i(xk_x+yk_y+zk_z)}\ dx\ dy\ dz\ . \tag{3c}$$

Equation (2) may then be solved formally for $F(k_x,k_y,k_z)$:

$$F(k_x,k_y,k_z) = \hat{F}(k_x,k_y,k_z)/H(k_x,k_y,k_z) \tag{4}$$

assuming $H(k_x,k_y,k_z) \neq 0$. The function $f(x,y,z)$ is then obtained from the inverse Fourier transform of $F(k_x,k_y,k_z)$. The practical problems associated with the implementation of this Fourier deconvolution method have been discussed extensively elsewhere[6,11] and will not be repeated here.

The function $\hat{f}(x,y,z)$ is represented as a three-dimensional grid of measured samples, and thus $\hat{F}(k_x,k_y,k_z)$ is obtained from the discrete Fourier transform of $\hat{f}(x,y,z)$. The function $h(x,y,z)$, however, can often be expressed in a simple algebraic form[10] such that eq. (3c) could be directly evaluated to yield a closed-form expression for $H(k_x,k_y,k_z)$. Such an expression would eliminate the need for numerical integration and offer greater flexibility to the Fourier deconvolution method.

Unfortunately, the evaluation of this integral is not always straightforward. The degree of difficulty depends on the angular limitations of the imaging system. Thus, if the point response function is zero outside a three-dimensional region denoted by Ω, eq. (3c) may be written:

$$H(k_x,k_y,k_z) = \iiint_{\Omega} h(x,y,z)\ e^{-2\pi i(xk_x+yk_y+zk_z)}\ dx\ dy\ dz\ . \qquad (5)$$

The integration is straightforward[12] for $\Omega \equiv 4\pi$, the full solid angle, but this does not correspond to a practically realizable system. Equation (5) has also been evaluated for the case of the circularly symmetric, rotating dual-detector positron camera[13]. In section 4 of this paper, eq. (5) will be evaluated for the more restrictive region imposed by a stationary detector system. First, however, it is necessary to provide an algebraic representation of the system response function.

3. THE SYSTEM POINT RESPONSE FUNCTION

The amplitude of the point response function, a distance r from an isotropic point source of unit strength, is given by the usual inverse square law:

$$h(x,y,z) = \frac{1}{4\pi r^2}\ , \qquad r^2 = x^2 + y^2 + z^2\ . \qquad (6)$$

For a limited angle, stationary system, the amplitude of the p.r.f. is given by eq. (6) within the acceptance cone of the system, and will be zero outside. The geometry of this cone will depend upon the geometry of the detectors, as shown in fig. 2 for detectors of square section.

If $\hat{f}(x,y,z)$ is constructed by back-projecting the projection data onto two-dimensional planes parallel to the detectors, an additional factor of cos θ is required to account for the angle (θ) between the perpendicular to the plane and the line joining any point on the plane to the point source. In this case, the appropriate p.r.f. is given by

$$h(x,y,z) = \frac{|\cos\theta|}{4\pi r^2} , \quad \cos\theta = \frac{z}{r} . \tag{7}$$

For the integration region Ω, cones of both circular and square sections are of interest, corresponding to the two types of detectors that have been used as stationary positron imaging devices -- the Anger camera (circular)[10,13] and the multiwire proportional chamber (square)[6,14]. The four functions of interest [eqs. (6) and (7) with square and circular sections] may be combined into one expression, as follows. Let the maximum acceptance angles in the xz and yz planes be ψ_1 and ψ_2 (fig. 2), respectively, and set

$$\alpha = \tan\psi_1 , \qquad 0 < \psi_1 < \frac{\pi}{2} ,$$

$$\beta = \tan\psi_2 , \qquad 0 < \psi_2 < \frac{\pi}{2} .$$

For n = 0,1 define the region Ω_n in three-dimensional space by

$$\Omega_n = \left\{(x,y,z) : \quad 0 \le |y| \le \beta|z| , \quad 0 \le \sqrt{x^2 + ny^2} \le \alpha|z|\right\}$$

with the convention that $\alpha = \beta$ if n = 1. Thus n = 0 corresponds to a cone of rectangular cross-section, and n = 1 to a cone of circular cross-section. The special case of a square section is found by taking $\alpha = \beta$ for n = 0.

For m = 0,1, define the function:

$$h_{m,n}(x,y,z) = \begin{cases} \dfrac{1}{4\pi} \dfrac{|z|^m}{(x^2 + y^2 + z^2)^{1+m/2}} & \text{for} \quad (x,y,z) \in \Omega_n \\ 0 & \text{otherwise} . \end{cases} \tag{8}$$

It is easy to see that the function $h_{0,n}(x,y,z)$ is identical to the function of eq. (6) within the region Ω_n, and the function $h_{1,n}(x,y,z)$ is identical to the function of eq. (7), again within the region Ω_n. Thus the four functions of interest are combined into the single expression of eq. (8).

4. EVALUATION OF THE FILTER, $H(k_x,k_y,k_z)$

Substituting eq. (8) into eq. (5), it is easy to verify that $H(k_x,k_y,k_z)$ is real, and can be written according to the notation introduced in the previous section as:

$$H_{m,n}(k_x,k_y,k_z) = \frac{1}{2\pi} \int_0^{\infty} \int_{-\beta z}^{+\beta z} \int_{-\sqrt{\alpha^2 z - n y^2}}^{\sqrt{\alpha^2 z - n y^2}} \frac{z^m}{(x^2 + y^2 + z^2)^{1+m/2}} \times \cos(xk_x + yk_y + zk_z)\, dx\, dy\, dz \,. \quad (9)$$

It can also be shown that $H_{m,n}(k_x,k_y,k_z)$ is an even function in the variables k_x, k_y, k_z, and thus it is sufficient to evaluate the integral (9) for k_x, k_y, $k_z \geq 0$.

Introduce ξ, η, ζ as integration variables and u, v, w as Fourier space variables by setting

$$x = \alpha\zeta\xi \,, \quad y = \beta\zeta\eta \,, \quad z = \zeta \,, \quad (10)$$

$$u = \alpha k_x \,, \quad v = \beta k_y \,, \quad w = k_z \,. \quad (11)$$

With the notation

$$R_{m,n}(u,v,w) = \frac{1}{\alpha\beta} H_{m,n}\left(\frac{u}{\alpha}, \frac{v}{\beta}, w\right) \quad (12)$$

and using eqs. (10) and (11), eq. (9) becomes

$$R_{m,n}(u,v,w) = \frac{1}{2\pi} \int_0^{\infty} \int_{-1}^{+1} \int_{-\sqrt{1-n\eta^2}}^{+\sqrt{1-n\eta^2}} \frac{\cos[(u\xi + v\eta + w)\zeta]}{(1 + \alpha^2\xi^2 + \beta^2\eta^2)^{1+m/2}} \, d\xi\, d\eta\, d\zeta \,. \quad (13)$$

Equation (13) is evaluated by considering the limit as $\gamma \to \infty$ of

$$R^{(\gamma)}_{m,n}(u,v,w) = \frac{1}{2\pi} \int_0^{\gamma} \int_{-1}^{+1} \int_{-\sqrt{1-n\eta^2}}^{+\sqrt{1-n\eta^2}} \frac{\cos[(u\xi + v\eta + w)\zeta]}{(1 + \alpha^2\xi^2 + \beta^2\eta^2)^{1+m/2}} \, d\xi\, d\eta\, d\zeta \,, \quad (14)$$

assuming always that $u^2 + v^2 + w^2 > 0$. Changing the order of integration in (14), and integrating with respect to ζ:

$$R^{(\gamma)}_{m,n}(u,v,w) = \frac{1}{2\pi} \int_{-1}^{+1} \int_{-\sqrt{1-n\eta^2}}^{+\sqrt{1-n\eta^2}} \frac{\sin\left[(u\xi + v\eta + w)\gamma\right] d\xi\, d\eta}{(u\xi + v\eta + w)(1 + \alpha^2\xi^2 + \beta^2\eta^2)^{1+m/2}} . \quad (15)$$

Now, for $u > 0$, let

$$t = u\xi + v\eta + w \quad \text{or} \quad \xi = \frac{1}{u}(t - v\eta - w) , \quad (16)$$

and substituting into (15),

$$R^{(\gamma)}_{m,n}(u,v,w) = \int_{-1}^{+1} \int_{a_n}^{b_n} g_m(t,\eta) \frac{\sin \gamma t}{t} dt\, d\eta , \quad (17)$$

where

$$g_m(t,\eta) = \frac{1}{2\pi u} \frac{1}{\left[1 + \frac{\alpha^2}{u^2}(t - v\eta - w)^2 + \beta^2\eta^2\right]^{1+m/2}} \quad (18)$$

$$a_n = v\eta + w - u\sqrt{1 - n\eta^2} , \quad (19)$$

$$b_n = v\eta + w + u\sqrt{1 - n\eta^2} . \quad (20)$$

Equation (17) may be written:

$$R^{(\gamma)}_{m,n}(u,v,w) = \int_{-1}^{1} \int_{a_n}^{b_n} \frac{g_m(t,\eta) - g_m(0,\eta)}{t} \sin \gamma t\, dt\, d\eta$$

$$+ \int_{-1}^{+1} g_m(0,\eta) \int_{a_n}^{b_n} \frac{\sin \gamma t}{t} dt\, d\eta . \quad (21)$$

According to the Riemann-Lebesgue lemma[15], the inner integration of the first double integral in eq. (21) vanishes for $\gamma \to \infty$. Using the sine integral,

$$\mathrm{Si}(x) = \int_0^x \frac{\sin y}{y}\, dy$$

with the property

$$\mathrm{Si}(\pm\infty) = \pm \frac{\pi}{2} ,$$

it can be shown that, as $\gamma \to \infty$, eq. (21) becomes

$$R_{m,n}(u,v,w) = \frac{1}{2} \int_{-1}^{+1} p_m(\eta) \left[\text{sign } (b_n) - \text{sign } (a_n) \right] d\eta , \tag{22}$$

where

$$p_m(\eta) = \frac{1}{2u} \frac{1}{\left[1 + \frac{\alpha^2}{u^2} (v\eta + w)^2 + \beta^2 \eta^2 \right]^{1+m/2}} . \tag{23}$$

Consider the indefinite integral,

$$P_m(\eta) = \int p_m(\eta)\, d\eta . \tag{24}$$

It can be easily verified that

$$p_m(\eta) = \frac{u^{1+m}}{2a^{1+m/2}} \frac{1}{\left[c + (\eta+b)^2 \right]^{1+m/2}} , \tag{25}$$

where

$$a = a(u,v) = \beta^2 u^2 + \alpha^2 v^2 , \tag{26}$$

$$b = b(u,v,w) = \frac{\alpha^2 vw}{a(u,v)} , \tag{27}$$

$$c = c(u,v,w) = \frac{u^2 \left[a(u,v) + \alpha^2 \beta^2 w^2 \right]}{a^2(u,v)} . \tag{28}$$

From (24) and (25), and using a table of standard integrals[16],

$$P_0(\eta) = \frac{u}{2a\sqrt{c}} \tan^{-1} \left(\frac{\eta + b}{\sqrt{c}} \right) , \tag{29}$$

$$P_1(\eta) = \frac{u^2}{2a^{3/2}c} \frac{\eta + b}{\sqrt{c + (\eta+b)^2}} . \tag{30}$$

Returning to eq. (22), let n = 0, and using eqs. (19) and (20):

$$a_0 = v\eta + w - u \ , \tag{31}$$

$$b_0 = v\eta + w + u \ . \tag{32}$$

An analysis of the straight lines (31) and (32) for the range $-1 \le \eta \le +1$, yields for the integral, eq. (22), the results for $u > 0$

$$R_{m,0}(u,v,w) = 0 \qquad \text{for} \quad 0 \le u + v < w \tag{33}$$

$$R_{m,0}(u,v,w) = P_m\left(\frac{u - w}{v}\right) - P_m(-1) \qquad \text{for} \quad v > 0, \quad |v-u| \le w \le |v+u| \tag{34}$$

$$R_{m,0}(u,v,w) = P_m\left(\frac{u - w}{v}\right) - P_m\left(-\frac{u + w}{v}\right) \qquad \text{for} \quad v \ge u > 0, \quad 0 \le w \le v - u \tag{35}$$

$$R_{m,0}(u,v,w) = P_m(1) - P_m(-1) \qquad \text{for} \quad u > v \ge 0, \quad 0 \le w \le u - v \tag{36}$$

For n = 1, eqs. (19) and (20) yield the curves

$$a_1 = v\eta + w - u\sqrt{1 - \eta^2} \ , \tag{37}$$

$$b_1 = v\eta + w + u\sqrt{1 - \eta^2} \ . \tag{38}$$

Analysis of these curves for the range $-1 \le \eta \le +1$ gives for the integral, eq. (22), again for $u > 0$,

$$R_{m,1}(u,v,w) = 0 \quad \text{for} \quad \sqrt{u^2 + v^2} < w \ , \tag{39}$$

$$R_{m,1}(u,v,w) = P_m\left(\frac{-vw + u\sqrt{u^2 + v^2 - w^2}}{u^2 + v^2}\right) - P_m\left(\frac{-vw - u\sqrt{u^2 + v^2 - w^2}}{u^2 + v^2}\right),$$

$$\text{for} \quad 0 \le w \le \sqrt{u^2 + v^2} \ . \tag{40}$$

Finally, for u = 0, v > 0, evaluating eq. (15) analogously to eqs. (16) to (22), the result is:

$$R_{m,n}(u,v,w) = 0 \qquad \text{for} \quad u = 0\ , \quad w > v > 0\ , \tag{41}$$

$$R_{m,n}(u,v,w) = \frac{1}{v} L_{m,n}\left(-\frac{w}{v}\right), \quad \text{for} \quad u = 0\ , \quad 0 \le w \le v\ , \tag{42}$$

where

$$L_{0,n}(\eta) = \frac{1}{\alpha\sqrt{1 + \beta^2\eta^2}} \tan^{-1}\left(\frac{\alpha\sqrt{1 - n\eta^2}}{\sqrt{1 + \beta^2\eta^2}}\right) \tag{43}$$

$$L_{1,n}(\eta) = \frac{1}{(1 + \beta^2\eta^2)} \frac{\sqrt{1 - n\eta^2}}{\sqrt{1 + \alpha^2(1-n\eta^2) + \beta^2\eta^2}}\ . \tag{44}$$

It remains, therefore, to express these results in terms of the original frequency space variables, k_x, k_y, k_z. Define

$$Q_m(\eta) = \alpha\beta\ P_m(\eta) \tag{45}$$

so that, from (29) and (30), after some manipulation,

$$Q_0(\eta) = \frac{1}{2k_3} \tan^{-1}\left(\frac{\beta k_2^2\eta + k_y k_z}{k_x \cdot k_3}\right), \tag{46}$$

$$Q_1(\eta) = \frac{k_2}{2k_3^2} \frac{\beta k_2^2\eta + k_y k_z}{\sqrt{k_x^2 k_3^2 + (\beta k_2^2\eta + k_y k_z)^2}}\ , \tag{47}$$

where

$$k_2^2 = k_x^2 + k_y^2 \tag{48}$$

$$k_3^2 = k_x^2 + k_y^2 + k_z^2 \tag{49}$$

are the two-dimensional and three-dimensional frequency space radii, respectively. Finally, using eqs. (12), (33) to (36), and (39) to (47),

$$H_{m,0}(k_x,k_y,k_z) = 0 \quad \text{for} \quad 0 \le \alpha k_x + \beta k_y < k_z\ , \ k_x \ge 0 \tag{50}$$

$$H_{m,0}(k_x,k_y,k_z) = Q_m\left(\frac{\alpha k_x - k_z}{\beta k_y}\right) - Q_m(-1)$$

$$\text{for} \quad k_x > 0, \quad k_y > 0, \quad |\beta k_y - \alpha k_x| \le k_z \le \alpha k_x + \beta k_y \tag{51}$$

$$H_{m,0}(k_x,k_y,k_z) = Q_m\left(\frac{\alpha k_x - k_z}{\beta k_y}\right) - Q_m\left(-\frac{\alpha k_x + k_z}{\beta k_y}\right)$$

$$\text{for} \quad \beta k_y > \alpha k_x > 0, \quad 0 \le k_z \le \beta k_y - \alpha k_x , \tag{52}$$

$$H_{m,0}(k_x,k_y,k_z) = Q_m(1) - Q_m(-1)$$

$$\text{for} \quad \alpha k_x > \beta k_y \ge 0, \quad 0 \le k_z \le \alpha k_x - \beta k_y , \tag{53}$$

$$H_{m,1}(k_x,k_y,k_z) = 0 \quad \text{for} \quad \alpha k_2 < k_z , \quad k_x \ge 0 , \tag{54}$$

$$H_{m,1}\left(k_x,k_y,k_z\right) = Q_m\left(\frac{-k_y k_z + k_x\sqrt{\alpha^2 k_2^2 - k_z^2}}{\alpha k_2^2}\right)$$

$$-Q_m\left(\frac{-k_y k_z - k_x\sqrt{\alpha^2 k_2^2 - k_z^2}}{\alpha k_2^2}\right)$$

$$\text{for} \quad 0 \le k_z \le \alpha k_2 , \quad k_x > 0 \tag{55}$$

$$H_{m,n}(k_x,k_y,k_z) = \frac{\alpha}{k_y} L_{m,n}\left(-\frac{k_z}{\beta k_y}\right), \quad k_x = 0 , \quad k_y > 0 , \quad 0 \le k_z \le \alpha k_2 \tag{56}$$

where Q_m is given by eqs. (46) and (47), $L_{m,n}$ by eqs. (43) and (44), and k_2^2 by eq. (48). This therefore completes the evaluation of a closed-form expression for the filter appropriate for use in eq. (4) with stationary detectors of either rectangular or circular cross-section. Note that the results could easily be generalized to detectors of elliptic section.

It has been suggested[9] that reconstructions can be improved by back-projecting with a weight proportional to some power of cos θ. This is incorporated into the above analysis by taking values of m other than 0 or 1, but it of course necessitates the evaluation of the corresponding indefinite integrals.

5. APPLICATION OF THE FILTER

Equations (50) to (56) have been evaluated for m = 0,1 at various values of (k_x,k_y,k_z) and compared with the standard numerical integration of eq. (9) in order to check, numerically, that the expressions are indeed equivalent. A discussion of the use of these filters with the reconstruction method outlined in section 2 is essentially beyond the scope of this paper, but for completeness some pictorial examples will be included. However, important details concerning the implementation of eq. (4) have been deliberately omitted, and may be found elsewhere[6].

A computer-generated phantom was used, consisting of a cylindrical shell containing a uniform sphere within which was located a smaller sphere, off-centre. The distribution of simulated positron activity for four transverse sections through this phantom is shown in fig. 3a. Annihilation events were simulated according to this activity distribution, for detectors of both square and circular cross-section. After back-projection of the annihilation events, the function $\hat{f}(x,y,z)$ on planes corresponding to those in fig. 3a are shown in fig. 3b for detectors of square section. Incorporating eqs. (50) to (53) and (56) into eq. (4), these images are filtered and the results shown in fig. 3c. The improvement in contrast and image clarity is obvious, as may be seen also from a profile through the phantom for the plane containing the high activity sphere ("tumour") (fig. 4). The same improvement is seen, using eqs. (54) to (56), for images with detectors of circular cross-section: the back-projected and filtered images are shown in figs. 5a and 5b, respectively, for the same phantom. A more detailed study will be the subject of a further publication.

Positron annihilation data from *in vivo* imaging with a pair of square-section, multiwire proportional chambers have been successfully reconstructed using the filter described by eqs. (50) to (53) and (56). A full description of the system, together with the images obtained, may be found elsewhere[14,17].

6. CONCLUSION

Filters for image reconstruction from a limited range of views are of interest for both transmission and emission computed tomography. In this paper, the derivation of a closed-form expression for some appropriate three-dimensional filters has been given, by evaluating analytically the Fourier transform of the system point response function within a region Ω. Closed-form expressions have the advantage of flexibility, and eliminate tedious numerical integration, with associated problems of precision and stability. Such expressions may be evaluated rapidly, and as required, during filtering, removing the need for precalculation and storage on some external device.

Acknowledgements

The authors thank Dr. A. Jeavons, CERN EP Division, for useful discussions, and one of us (D.T.) gratefully acknowledges Prof. A. Donath, Dept. of Nuclear Medicine, Cantonal Hospital, Geneva, for his support and encouragement.

REFERENCES

1. Budinger TF, Gullberg GT: Transverse section reconstruction of gamma-ray emitting radionuclides in patients. (In) Reconstruction Tomography in Diagnostic Radiology and Nuclear Medicine, ed. by MM Ter-Pogossian, ME Phelps, GL Brownell, JR Cox, DO Davis and RG Evens, University Park Press, pp 315-342, 1977

2. Jaszczak RJ, Chang LT, Stein NA, Moore FE: Whole-body single-photon emission computed tomography using dual, large-field-of-view scintillation cameras. Phys. Med. Biol. 24:1123-1143, 1979

3. Kak A: Computerized tomography with X-ray, emission and ultrasound sources. Proc. of the IEEE 67, No. 9:1245-1271, 1979

4. Phelps ME: Emission computed tomography. Sem. Nucl. Med. 7:337-365, 1977

5. Pelc NJ, Chesler DA: Utilization of cross-plane rays for three-dimensional reconstruction by filtered back-projection. J. Comput. Assist. Tomogr. 3:385-395, 1979

6. Townsend D, Schorr B, Jeavons A: Three-dimensional image reconstruction for a positron camera with limited angular acceptance, to appear in IEEE Trans. Nucl. Sci. NS-27, 1980

7. Budinger TF, Gullberg GT: Three-dimensional reconstruction in nuclear medicine emission imaging. IEEE Trans. Nucl. Sci. NS-21: 2-20, 1974

8. Brooks RA, DiChiro G: Principles of computer assisted tomography (CAT) in radiographic and radioisotopic imaging. Phys. Med. Biol. 21:689-732, 1976

9. Chu G, Tam KC: Three-dimensional imaging in the positron camera using Fourier techniques. Phys. Med. Biol. 22:245-265, 1977

10. Atkins FB, Muehllehner G, Harper PV: Positron emission computed tomography using large area detectors. In: Proc. of 5th Int. Conf. on Information Processing in Medical Imaging, Nashville, Tenn.:pp 195-213, 1977

11. Tam KC, Perez-Mendez V, Macdonald B: Limited angle 3-D reconstructions from continuous and pinhole projections, to appear in IEEE Trans. Nucl. Sci. NS-27, 1980

12. Tanaka E: Generalized correction functions for convolutional techniques in three-dimensional image reconstruction. Phys. Med. Biol. 24:157-161, 1979

13. Colsher JG: Fully three-dimensional positron emission tomography. Phys. Med. Biol. 25:103-115, 1980

14. Jeavons A: The CERN proportional chamber positron camera. In: Proc. 5th Int. Conf. Positron Annihilation, Lake Yamanaka, Japan, pp 355-370, 1979

15. Apostol TM: Mathematical Analysis, Addison-Wesley, Reading, Mass., 1975:Section 15-6

16. Gradshteyn IS and Ryzhik IM: Tables of Integrals, Series and Products. Academic Press, New York, 1965: p 83

17. Jeavons A, Kull K, Lindberg B, Lee L, Townsend D, Frey P, Donath A: A proportional chamber positron camera for medical imaging. To be presented at the Wire Chamber Conference, Vienna, 1980

Figure captions

Fig. 1 : Coincidence detection of photon pairs from electron-positron annihilation.

Fig. 2 : The acceptance cone for the point response function with detectors of square section.

Fig. 3 : a) Distribution of annihilation events on four sections through a computer-generated phantom.

b) The back-projected distributions for detectors of square section. Same phantom cross-sections as fig. 3a.

c) The corresponding images after filtering.

Fig. 4 : A profile through the region containing the high activity sphere ("tumour").

Fig. 5 : a) Same as fig. 3b, but for detectors of circular section.

b) The corresponding images after filtering.

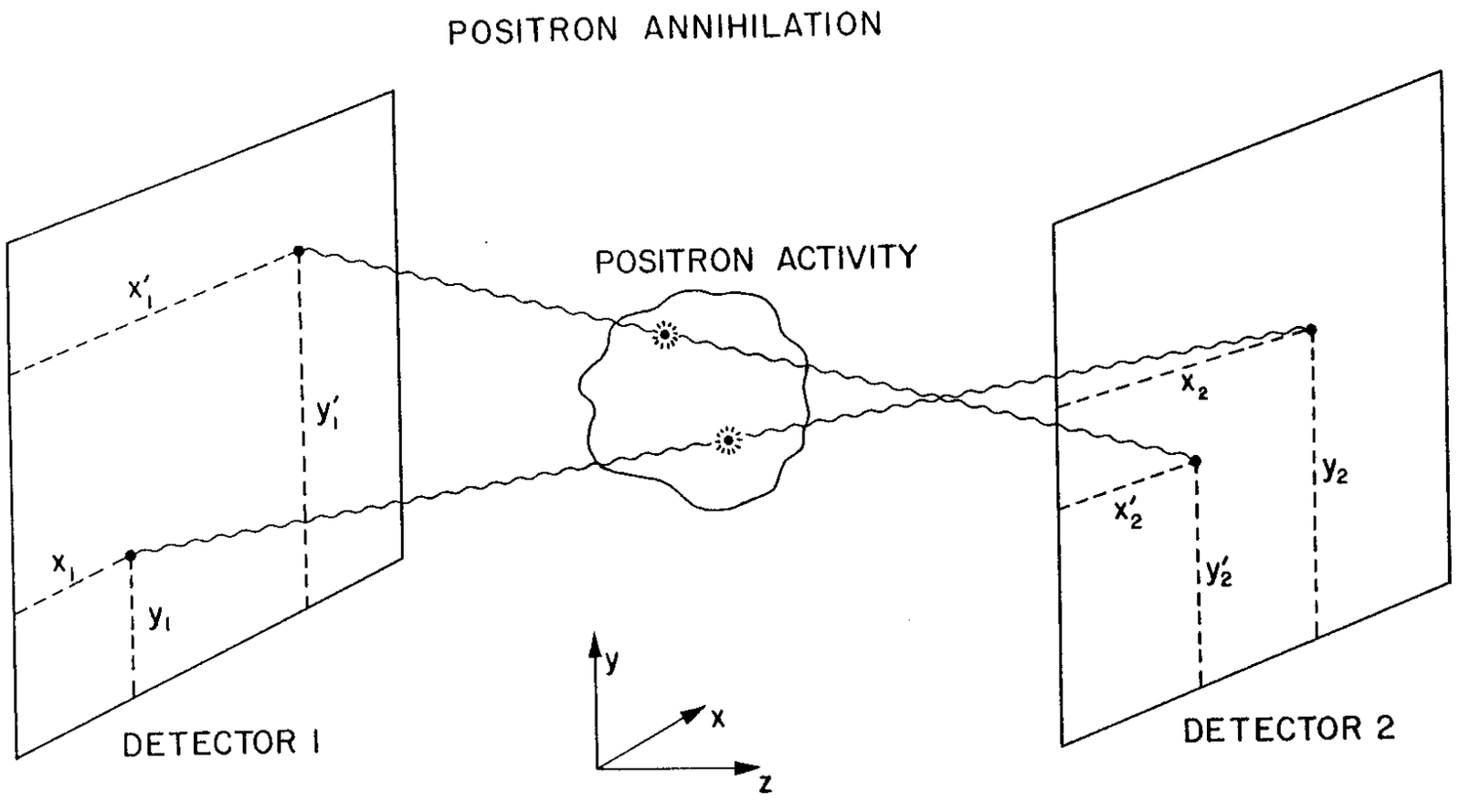

POSITRON ANNIHILATION
POSITRON ACTIVITY
x'_1
y'_1
x_1
y_1
DETECTOR 1
y
x
z
x_2
y_2
x'_2
y'_2
DETECTOR 2

Fig. 1

POINT RESPONSE FUNCTION

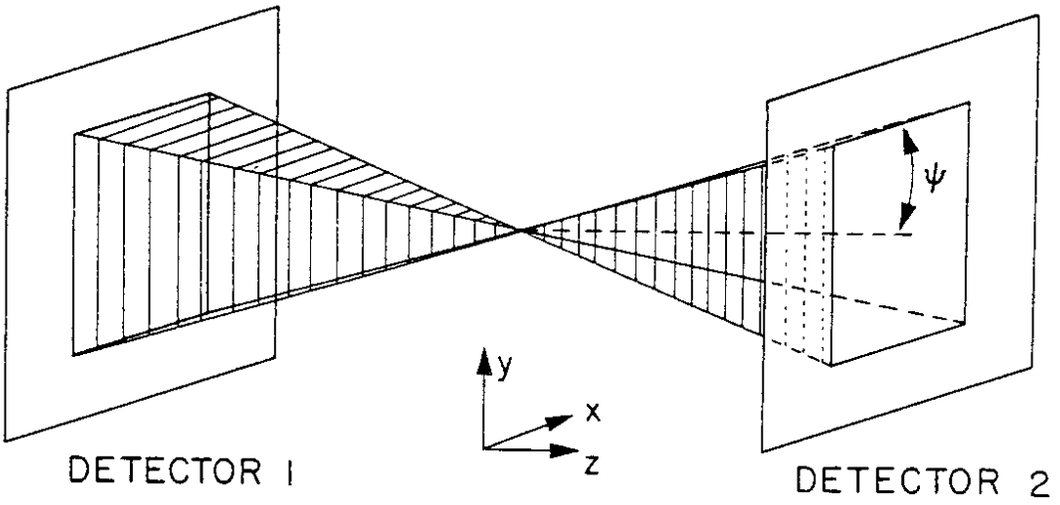


Fig. 2

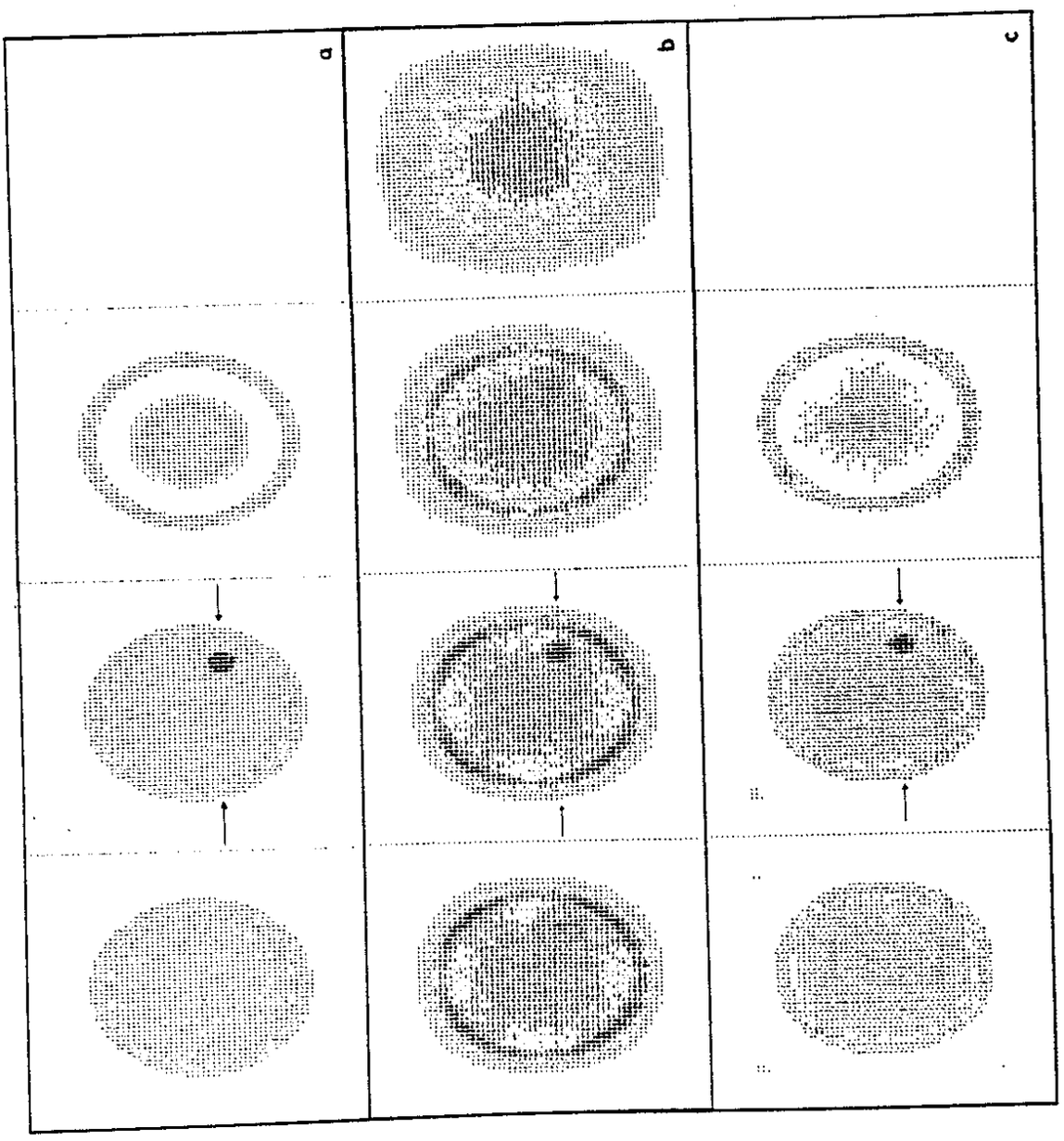


Fig. 3

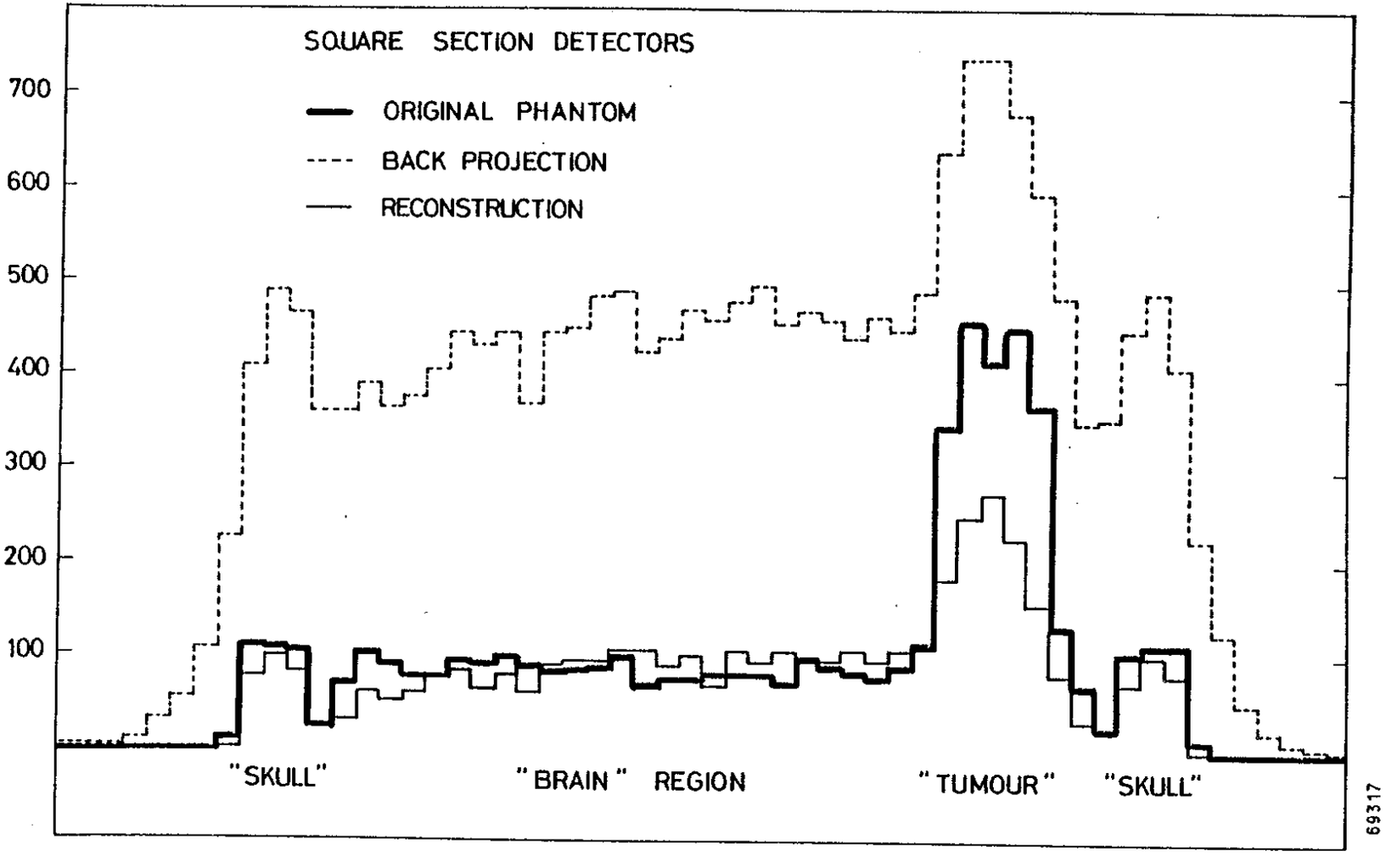

SQUARE SECTION DETECTORS
ORIGINAL PHANTOM
BACK PROJECTION
RECONSTRUCTION
700
600
500
400
300
200
100
"SKULL"
"BRAIN" REGION
"TUMOUR"
"SKULL"
69317

Fig. 4

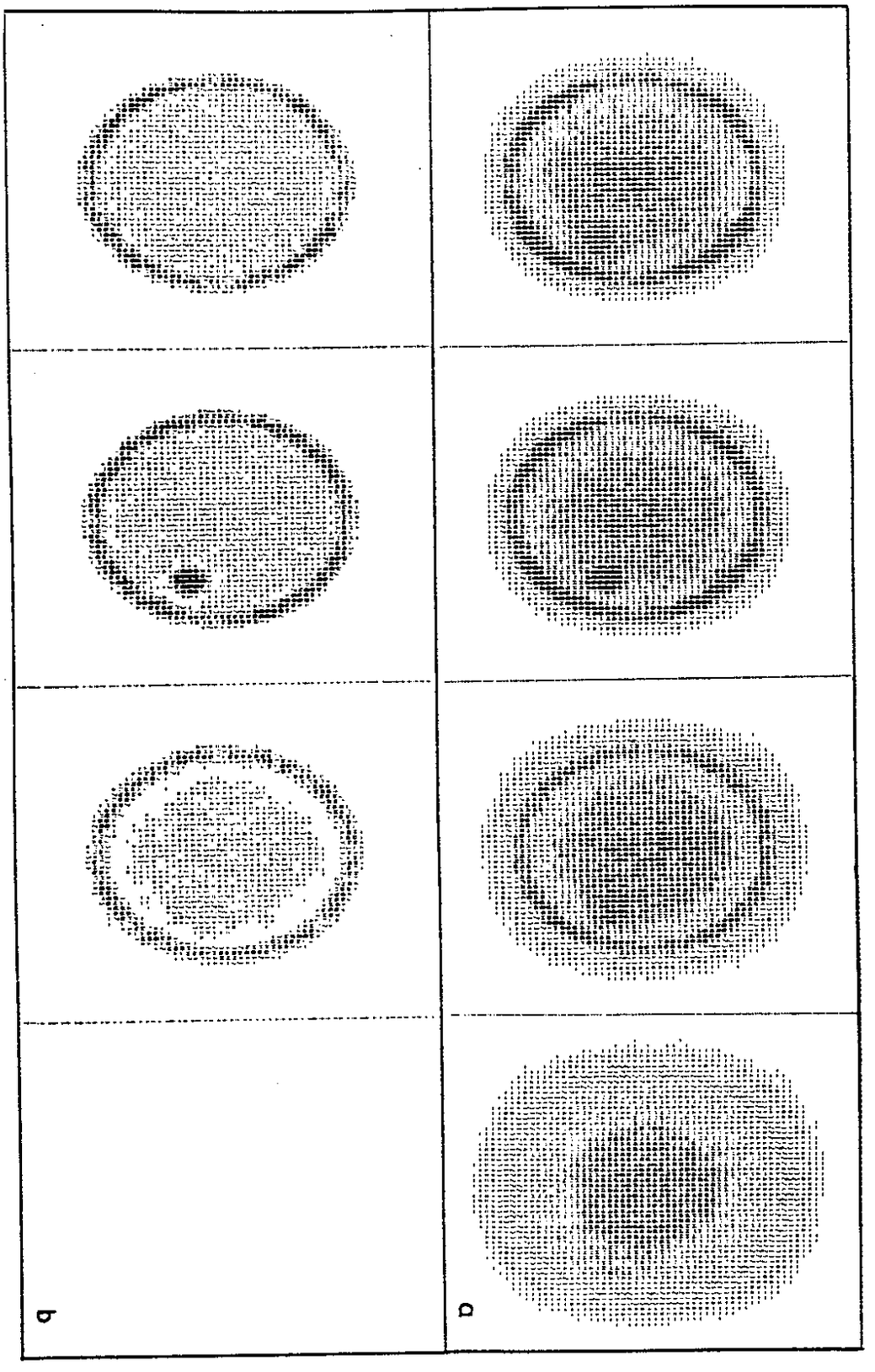


Fig. 5